

1 **Cloud activation properties of aerosol particles**

2 **in a continental central European urban environment**

3 Imre SALMA¹, Wanda THÉN², Máté VÖRÖSMARTY², and András Zénó GYÖNGYÖSI¹

4 ¹Institute of Chemistry, Eötvös Loránd University, Budapest, Hungary

5 ²Hevesy György Ph. D. School of Chemistry, Eötvös Loránd University, Budapest, Hungary

6 *Correspondence to:* Imre Salma (salma.imre@ttk.elte.hu)

7 **Abstract.** Collocated measurements by condensation particle counter, differential mobility particle sizer
8 and cloud condensational nuclei counter instruments were realised in parallel in central Budapest from
9 15 April 2019 to 14 April 2020 to gain insight into the cloud activation properties of urban aerosol
10 particles. The median total particle number concentration was $10.1 \times 10^3 \text{ cm}^{-3}$. The median concentrations
11 of cloud condensation nuclei (CCN) at water vapour supersaturations (S_s) of 0.1, 0.2, 0.3, 0.5 and 1.0 %
12 were 0.59, 1.09, 1.39, 1.80 and $2.5 \times 10^3 \text{ cm}^{-3}$, respectively. They represented from 7 to 27 % of the total
13 particles. The CCN concentrations were considerably larger, whereas the activation fractions were
14 substantially and systematically smaller than for regional or remote locations. The effective critical dry
15 particle diameters ($d_{c,\text{eff}}$) were derived utilising the CCN concentrations and particle number size
16 distributions. Their medians were 207, 149, 126, 105 and 80 nm, respectively. They were positioned
17 within the accumulation mode of the typical particle number size distribution. Their frequency
18 distributions revealed a single peak, which geometric standard deviation increased monotonically with S .
19 The broadening indicated large time variability in the activation properties of smaller particles. The
20 frequency distributions also showed a fine structure. Its several compositional elements seemed to change
21 in a tendentious manner with S . The relationships between the critical S and $d_{c,\text{eff}}$ suggested that the urban
22 aerosol particles in Budapest with a diameter larger than approximately 130 nm showed similar
23 hygroscopicity than the continental aerosol in general, whereas the smaller particles were less hygroscopic
24 than that. Seasonal cycling of the CCN concentrations and activation fractions implied modest alterations
25 and for the larger S_s only. They likely reflected the changes in particle number concentrations, chemical
26 composition and mixing state of particles as well. The seasonal dependencies for $d_{c,\text{eff}}$ were featureless,
27 which indicated that the urban particles exhibited more or less similar droplet activation properties over
28 the year. This is again different from non-urban locations. The hygroscopicity parameters (κ values) were
29 computed without determining time-dependent chemical composition of particles. Their medians were
30 0.15, 0.10, 0.07, 0.04 and 0.02, respectively. The averages suggested that the larger particles exhibited
31 considerably higher hygroscopicity than the smaller particles. We found that the urban aerosol showed
32 substantially smaller κ values than for regional or remote locations, which were reported previously. All
33 these could be virtually linked to specific source composition of particles in cities. The relatively large
34 variability in the hygroscopicity parameter sets for a given S emphasized that their individual values

35 represented the CCN population in the ambient air, while the averages stood mainly for the particles with
36 a size close to the effective critical dry particle diameters.

37 **1 Introduction and objectives**

38 Water is the most abundant vapour in the troposphere. Its condensation onto aerosol particles is the only
39 relevant pathway for cloud or fog droplet formation at water vapour supersaturations (S_s) occurring in the
40 ambient air (Pruppacher and Klett, 2000). The S_s in clouds are usually less than 1 % with a median value
41 between 0.1 and 0.2 %. The number and size of the generated droplets depend both on particle properties
42 and actual local S (Andreae and Rosenfeld, 2008). Only a subset of aerosol particles are able to grow to
43 droplets at a given S ; they are called cloud condensation nuclei (CCN) for this S . From the aerosol side,
44 this ability is primarily controlled by the size of particles and to a lesser degree by their chemical
45 composition and mixing state (Dusek et al., 2006). The S_s are mainly governed by cloud dynamics and
46 also by existing cloud droplets. The latter property acts as a sink of water vapour and depends on CCN
47 concentrations as well. Different updraft velocities and droplet populations in clouds result in different
48 S_s , which can also change the activation process. As a consequence, the droplet formation can be limited
49 by the availability of CCN and/or updraft velocities. The former case ordinarily prevails in the global
50 troposphere at concentrations of $<9 \times 10^3 \text{ cm}^{-3}$ and is called CCN-limited regime (Rosenfeld et al., 2014).

51
52 The CCN modify the intensity and other properties of the sunlight reaching the Earth's surface indirectly
53 through cloud droplets. It is achieved primarily through the droplet number, droplet size and cloud
54 residence time (Andreae and Rosenfeld, 2008; Rosenfeld et al., 2008, 2014). They also influence the
55 hydrological cycle including the precipitation amount and intensity, the vegetation and its interactions
56 with the carbon cycle as well as the atmospheric chemistry, physics and dynamics. Moreover, it is this
57 indirect effect of aerosols that has the most uncertain contribution to the global radiative forcing
58 calculations (e.g. Carslaw et al., 2013). This is particularly important since the number concentrations of
59 particles seem to be increasing globally due to anthropogenic activities (Andreae et al., 2005).
60 Concentrations of CCN can vary considerably in space and time. Dedicated studies have been performed
61 in field experiments at several locations in the world and at various laboratories (e.g. Dusek et al., 2006;
62 McFiggans et al., 2006; Hudson, 2007; Rose et al., 2008, 2010; Kuwata and Kondo, 2008; Pringle et al.,
63 2010; Wex et al., 2010; Burkart et al., 2011; Sihto et al., 2011; Jurányi et al., 2011; Kerminen et al., 2012;
64 Topping and McFiggans, 2012; Paramonov et al., 2015; Herenz et al., 2018; Schmale et al., 2018). Despite
65 their importance, our knowledge on aerosol–water vapour interactions at supersaturations typical for
66 atmospheric conditions and on cloud microphysics have remained still insufficient. Longer-term studies
67 (for instance, of 1 year) are preferred to understand these processes and their consequences. A broad
68 regional coverage is also desired to reach representative results. The data sets for the environmental
69 category of large cities are particularly scarce.

70

71 The study presented here deals with the cloud droplet activation properties of aerosol particles in a
72 continental central European city, Budapest. It has 2.2 million inhabitants in the metropolitan area, and it
73 is the largest city in the Carpathian Basin. Online aerosol and meteorological measurements have been
74 going on in a semi-continuous manner at the Budapest platform for Aerosol Research and Training
75 (BpART) Laboratory for more than a decennium (Salma et al., 2011; Mikkonen et al., 2020). The related
76 essential instruments include a differential mobility particle sizer (DMPS) and a condensation particle
77 counter (CPC). They were complemented by a continuous-flow cloud condensation nuclei counter
78 (CCNc) in 2018. The combinations of the long-term particle number size distributions, total particle
79 number concentrations and CCN data at various *S*s facilitate the utilisation of special methods for the data
80 validation and of joint evaluation procedures.

81

82 The major objective of the present study is to gain insight into the cloud activation properties of urban
83 aerosol particles based on 1 measurement year in central Budapest. Specifically, we report, discuss,
84 explain and interpret here the measured time series and descriptive statistics of CCN concentrations, the
85 activated fractions of aerosol particles, the effective activation dry particle diameters, the effective
86 hygroscopicity parameters under various supersaturated conditions and formulate some common
87 consequences of the data sets.

88 **2 Methods**

89 The time interval considered in this study was from 15 April 2019 to 14 April 2020. The number of days
90 with the CPC, DMPS, CCNc and meteorological measurements covered 100, 99, 85 and 100 % of the
91 relevant days, respectively. The CCNc was out of operation in January 2020. It is mentioned only for
92 completeness that the overall interval also involved the emergency phase (from 12 to 27 March 2020, 16
93 d) and the restriction on movement phase (from 28 March to the end of the measurement year, 18 d) of
94 the first outbreak of the COVID-19 pandemic in Hungary (Salma et al., 2020b). Local time (LT=UTC+1
95 or daylight-saving time, UTC+2) was chosen as the time base of the data because it was observed that the
96 daily activity time pattern of inhabitants largely influences many atmospheric processes in cities (Salma
97 et al., 2014; Mikkonen et al., 2020).

98 **2.1 Experimental part**

99 All measurements were performed at the BpART Laboratory (N 47° 28' 30", E 19° 3' 45", 115 m above
100 mean sea level) of the Eötvös Loránd University (Salma et al., 2016). It represents an average atmospheric
101 environment for central Budapest due to its geographical location and meteorological conditions. Thus,
102 it can be regarded as an urban background site. The local sources comprise residential and household
103 emissions including seasonal heating, exhaust of vehicle traffic and some industrial sources (Salma et al.,

104 2017, 2020a, 2020b). Long-range transport of air masses can also play a role in shorter time intervals.
105 The measurement site is located 85 m from the river Danube. The sampling inlets of the instruments were
106 set up at heights between 12 and 13 m above the street level. Weather shield and insect net were only
107 adopted to them. The laboratory was air conditioned at 20 ± 3 °C.

108
109 The CPC instrument deployed (TSI, model 3752, USA) was operated with an aerosol inlet flow of 1.5 L
110 min^{-1} , and recorded concentrations of particles with a diameter above 4 nm using n-butanol as a working
111 fluid. Its sampling inlet was made of stainless-steel tube with a diameter of 6.35 mm ($\frac{1}{4}$ inch) and length
112 of ca. 1.6 m. Mean particle number concentrations (N_{CPC}) with a time resolution of 1 min were extracted
113 from its extended data base. The nominal specification of the CPC warrants an agreement in
114 concentrations better than ± 10 % between two identical instruments operating in the single-particle
115 counting mode with a data averaging interval of >30 s.

116
117 The DMPS system utilised was a laboratory-made flow-switching-type device (University of Helsinki,
118 Finland). It measured particle number concentrations in an electrical mobility diameter range from 6 to
119 1000 nm in the dry state of particles (with a relative humidity of $\text{RH} < 30$ %) in 30 channels with a time
120 resolution of 8 min (Salma et al., 2011, 2016). Its main components included a radioactive (^{60}Ni) bipolar
121 diffusion charger, a monotube Nafion semi-permeable membrane dryer, a 28-cm-long Vienna-type
122 differential mobility analyser and a butanol-based CPC (TSI, model 3775). The aerosol flow in the high
123 and low modes were 2.0 and 0.31 L min^{-1} , respectively. The sheath flows were 10 times larger than the
124 aerosol flows. The sampling inlet was made of copper tube with a diameter of 6 mm and length of ca. 1.9
125 m. The measurements were realised semi-continuously according to international technical standards
126 (Wiedensohler et al., 2012; Schmale et al., 2017).

127
128 The CCNc system implemented was a DMT-200 instrument (Droplet Measurement Technologies, USA).
129 It contains two vertical condensation chambers A and B of cylindrical shape (inner diameter 2.3 cm,
130 length 50 cm; Roberts and Nenes, 2005; Rose et al., 2008). Their porous internal walls are continuously
131 wetted with liquid water from peristaltic pumps. A linear positive temperature gradient along the cylinders
132 is established and controlled at the top, middle and bottom zones of the chambers. The aerosol sample
133 flow is continuously guided through the centre of the chambers and is surrounded by filtered sheath air
134 flow. The flows proceed from top to bottom under laminar conditions and near-ambient air pressure (P).
135 As the flows pass through the chambers, heat and water vapour are transported from the internal wall
136 surface towards the centre of the chambers. Because water molecules diffuse faster than the air molecules
137 (transferring the heat), a constant water vapour S is generated along the axes. Various S s can be adjusted
138 by selecting different temperature gradients. The particles are exposed to this S for ca. 10 s. Those particles
139 that activate at a critical S lower than the adjusted value form droplets. Their size is substantially larger

140 than for inactivated particles. The droplets are detected at the exit of the chambers by optical particle
141 counters as size distributions in a diameter range from 0.75 to 10 μm . The droplets larger than 1 μm are
142 considered to be activated CCN, whereas the concentration of particles in this size interval is negligible.

143

144 The total air flow rates were set to $500 \text{ cm}^3 \text{ min}^{-1}$ and the ratio of the sample flow rate to the sheath flow
145 rate was 1:10. The selected S s were 0.1, 0.2, 0.3, 0.5 and 1.0 % stepping from the lowest to the highest
146 values within a measuring cycle with duration times of 12, 5, 5, 5 and 5 min, respectively. The data
147 measured by the system were recorded every 1 s. The CCN concentrations at a given S ($N_{\text{CCN},S}$) obtained
148 by the two chambers should not differ by more than 15 %. The system was run in polydisperse operation
149 mode largely according to the ACTRIS standard operation protocol (Gysel and Stratmann, 2013).

150

151 The meteorological measurements took place on site of the BpART Lab. Air temperature (T), RH, wind
152 speed (WS), wind directions (WD), P and global solar radiation (GRad) were obtained by standardised
153 meteorological sensors (HD52.3D17, Delta OHM, Italy and SMP3 pyranometer, Kipp and Zonen, the
154 Netherlands) with a time resolution of 1 min as supporting information.

155 **2.2 Data treatment and validation**

156 The measured DMPS data were inverted into discrete size distributions, which were utilised to calculate
157 particle number concentrations in the diameter ranges from 6 to 25 nm (N_{6-25}), from 6 to 100 nm (N_{6-100}),
158 from 30 to 1000 nm ($N_{30-1000}$) and from 6 to 1000 nm (N_{6-1000}). The size intervals were selected to
159 represent various important source types of particles and to maintain the comparison with earlier results.
160 The extraction, treatment and processing of the measured CCNc data including the date and time, $N_{\text{CCN},S}$,
161 flow rates and activation temperatures ($T_a=(T_1+T_2)/2$, with T_1 and T_2 as the read wall temperatures at the
162 top and middle zones of the condensation chambers; Gysel and Stratmann, 2013) were accomplished for
163 each S stage by a laboratory-developed computer software AeroSoLutions.

164

165 The averaging of the individual measured data was performed from the end of each S stage in a backward
166 direction over a set time span within the temperature stability of the condensation chambers. The
167 averaging times were determined by examining several randomly selected time-dependencies of CCN
168 concentrations and temperatures in different seasons. The averaging intervals can be preselected for each
169 S , and were ordinarily set to 90, 210, 210, 180 and 150 s, respectively for S s of 0.1, 0.2, 0.3, 0.5 and 1.0
170 %. Their proper functioning was monitored within the data treatment, and they were refined for some
171 individual cases if it was necessary. Warning flags on suspicious data were generated in the data
172 processing, and the filtered data were checked separately. The two data sets for chambers A and B were
173 averaged if their ratio was $<20\%$. Otherwise, one of the two data sets was chosen on the basis of their
174 time evolution. For the S of 0.1 % (for small CCN concentrations), another averaging criterion, namely

175 $ABS(N_{CCN,A}-N_{CCN,B})/\min(SD_{CCN,A}, SD_{CCN,B}) < 5$ was utilised instead of the concentration ratio. The limits
176 were based upon exercises with concentrations in ordinary measurement intervals. They represent
177 sensible and pragmatic approaches, although alternative thresholds could also be set. Finally, it was
178 checked that the averaged CCN concentrations increased monotonically with S within the measurement
179 cycles. The time resolution of all experimental data derived from the CCNc instrument was 32 min.

180

181 The N_{6-1000} data from the DMPS system were compared to the CPC concentrations, which were averaged
182 over the corresponding DMPS measuring cycle. Due to the differences in the lowest measurable diameters
183 (6 vs. 4 nm, respectively), an agreement between the two instruments can be expected if the contribution
184 of nucleation-mode particles to total number of particles is negligible. Additional factors such as larger
185 particle transport losses along their longer path in the DMPS system and possibly different response times
186 of the two CPCs involved in the instruments could also contribute to the observed concentration
187 discrepancy (Salma et al., 2016). The comparison was realised by evaluating the N_{CPC}/N_{6-1000} ratio as a
188 function of the N_{6-30}/N_{6-1000} ratio. The intercept of their regression line was considered as the correction
189 factor for the DMPS system (Sect. 3.1).

190

191 For validation purposes, the CCN concentrations at the S of 1.0 % ($N_{CCN,1.0\%}$) were compared to the
192 particle number concentrations. The two concentrations are expected to be similar if most particles
193 activate at this S . In a previous survey, certain criteria were set to exclude the time intervals when very
194 small, hence, non-activating particles are present in larger concentrations (Schmale et al., 2017). The
195 comparison was performed under the conditions when the concentration ratio of particles < 30 nm to the
196 total particles was < 10 % or between 10 and 20 %. These criteria were successfully adopted for remote
197 or regional locations. However, the conditions seem not to be applicable for urban data sets since their
198 annual $N_{30-1000}/N_{6-1000}$ means and standard deviations (SDs) are low with respect to more distant
199 environments. In Budapest, for instance, they were (52 ± 15) %. This also caused that the relative number
200 of the DMPS data fulfilling either the criterium 1 or 2 above was very small, i.e. only 2 % on a yearly
201 scale. This is due to relatively large and persistent contributions of high-temperature emission sources of
202 particles typically present in cities. The representativity of any conclusion for the whole data set derived
203 on the basis of such limited cases could to be statistically questioned.

204

205 To avoid this weak point, we propose here another criterium for urban or polluted environments as a
206 compromise between the larger relative number of cases and the constrained contribution of small, thus
207 non-activating particles. The $N_{CCN,1.0\%}$ data are only compared to the $N_{30-1000}$ data if the corresponding
208 ratio of $N_{30-1000}/N_{6-1000} > 70$ %. This was fulfilled in a larger number of the DMPS concentrations and
209 yielded more robust statistics, while the contribution of smaller particles remained still higher than for the
210 original criteria. The limit value of 70% was determined in a pragmatic manner to express this

211 compromise. Alternative values could also be set. The size distribution spectrum which date and time was
212 the closest (within 20 min) and smaller than or equal to that of the CCN concentration was considered.
213 The procedure is further discussed in Sect. 3.1.

214 **2.3 Particle hygroscopicity**

215 For atmospheric aerosol, the activated fraction of particles tends to increase gradually with the dry particle
216 diameter (as a sigmoid function instead of a step function valid for internally mixed monodisperse
217 particles). This is primarily due to the fact that atmospheric particles are often external mixtures, or their
218 chemical composition changes with particle size (Dusek et al., 2006; Rose et al., 2010). A threshold
219 activation diameter, which is called effective critical dry particle diameter ($d_{c,eff}$) is defined in these cases
220 as the size at which 50 % of the dry particles activate at a given S (Rose et al., 2008, 2010).

221
222 The effective critical dry particle diameters were assessed from collocated polydisperse CCN and particle
223 number size distribution measurements as (Sihto et al., 2011; Kerminen et al., 2012; Schmale et al., 2018):

$$224 \quad N_{CCN,S} = \sum_{i=d_{c,eff}}^{d_{max}} N_i, \quad (1)$$

225 where d_{max} is the largest dry particle diameter measured by the sizing instrument (here DMPS) and N_i is
226 the number of particles in the size channel i of the instrument. Hence, the concentrations were summed
227 from the largest particle size (d_{max}) towards the smaller diameters until the measured CCN concentration
228 was obtained. In order to estimate the $d_{c,eff}$ with higher accuracy, a logarithmic interpolation was
229 accomplished between the last 2 diameters of the summation. The size distribution spectrum which date
230 and time was the closest (with 20 min) and smaller than or equal to that of the CCN concentration was
231 considered.

232
233 It has to be noted that the assumption of internally mixed particles is rarely met in urban environments
234 including Budapest (Enroth et al., 2018). However, the approximation involves largely compensating
235 influences, which still lead to reasonable results (Kammermann et al., 2020).

236
237 The cloud droplet activation of aerosol particles refers to their indefinite diameter growth (i.e. up to the
238 droplet sizes) due to condensation of water vapour at constant saturation ratio ($s=p/p_0$ with p being the
239 partial vapour pressure of water over a droplet solution and p_0 being the saturation vapour pressure of
240 water over pure water with a flat surface). The conditions for the S_{eq} (with $S=s-1$) at which the droplets
241 stay in equilibrium with the water vapour can be described by the Köhler model (e.g. Pruppacher and
242 Klett, 2000; McFiggans et al., 2006). To calculate the composition-dependent S_{eq} as function of the
243 droplet diameter (d_{wet}) for a given dry particle diameter d_s , most controlling variables are further
244 simplified and approximated within different types of thermodynamic parametrisations. In the present

245 study, the effective hygroscopicity model was adopted (Petters and Kreidenweis, 2007). Laboratory and
 246 field measurements together with modelling considerations have indicated that this parametrisation
 247 proved to be a reliable under both sub- and supersaturation conditions (Rose et al., 2008; Merikanto et
 248 al., 2009; Rissler et al., 2010; Sihto et al., 2011; Kerminen et al., 2012; Schmale et al., 2018).

249
 250 The S_{eq} can be expressed by assuming volume additivity of solute and water in the droplet and spherical
 251 shapes of the dry solute particle and solution droplet as (Petters and Kreidenweis, 2007):

$$252 \quad S_{\text{eq}} = \frac{d_{\text{wet}}^3 - d_s^3}{d_{\text{wet}}^3 - d_s^3 (1 - \kappa)} \exp\left(\frac{A}{d_{\text{wet}}}\right) - 1, \quad (2)$$

253 where

$$254 \quad A = \frac{4\sigma_{\text{d/a}}M_w}{RT\rho_w}. \quad (3)$$

255 The κ , $\sigma_{\text{d/a}}$, M_w , ρ_w , R and T are the hygroscopicity parameter, surface tension of the droplet–air interface,
 256 molar mass of water ($0.018015 \text{ kg mol}^{-1}$), density of water, the universal gas constant ($8.3145 \text{ J mol}^{-1} \text{ K}^{-1}$)
 257 and absolute temperature of the droplet and air in the thermodynamic equilibrium, respectively. The
 258 $\sigma_{\text{d/a}}$ was assumed to be that of pure water. Some organic chemical species in atmospheric aerosol particles
 259 such as humic-like substances are surface active and can lower the surface tension of the droplets
 260 (Facchini et al., 1999; Ovadnevaite et al., 2017). This depression is mainly controlled by diffusion of
 261 surfactants from the bulk of the droplet to its surface. It takes several hours to reach the thermodynamic
 262 equilibrium at medium concentrations (Salma et al., 2006). This implies that the possible alterations
 263 related to the lower surface tension than for the water are small with respect to estimated experimental
 264 uncertainties and can also be compensated by some surface/bulk partitioning effects (Sorjama et al.,
 265 2004). The surface tension of pure water seems, therefore, to be a reasonable approximation to reality
 266 under the conditions considered in the present study.

267
 268 The κ values can be computed by solving Eq. 2. This contains several independent variables, i.e. T , d_s
 269 and d_{wet} in addition to the S_{eq} and κ value. The S_s are controlled by the CCNc instrument; the T can be
 270 expressed by the activation temperature in the condensation chamber (T_a , Sect. 2.2). For polydisperse
 271 atmospheric aerosol, d_s can be approximated by $d_{\text{c,eff}}$ (Eq. 1; Rose et al., 2008). An additional independent
 272 relationship, namely the fact that the dependency of S_{eq} on variable d_{wet} exhibits a maximum (of S_c at a
 273 diameter of d_c) is also exploited for solving Eq. 2. The κ values were computed in an iterative manner by
 274 varying both κ and d_{wet} until the calculated S_s were equivalent to the adjusted S_s and at the same time, it
 275 showed a maximum (Jurányi et al., 2010; Rose et al., 2010).

276

277 When the volume occupied by the solute can be neglected with respect to the water volume at the stage
278 of activation, the S_c can be approximated for $\kappa > 0.2$ by (Petters and Kreidenweis, 2007):

$$279 \ln(S_c) = \sqrt{\frac{4A}{27} \frac{1}{\kappa d_c^3}}. \quad (4)$$

280

281 The time resolution of all modelled data was 32 min, which resulted in the total counts of data sets
282 typically 13.6×10^3 at each S level.

283 3 Results and discussion

284 The relevant meteorological properties for each month are summarised in Table S1 in the Supplement to
285 assist in creating the first impression on the actual atmospheric environment. They also indicate usual
286 weather conditions in Budapest during the measurement year without extraordinary situations.

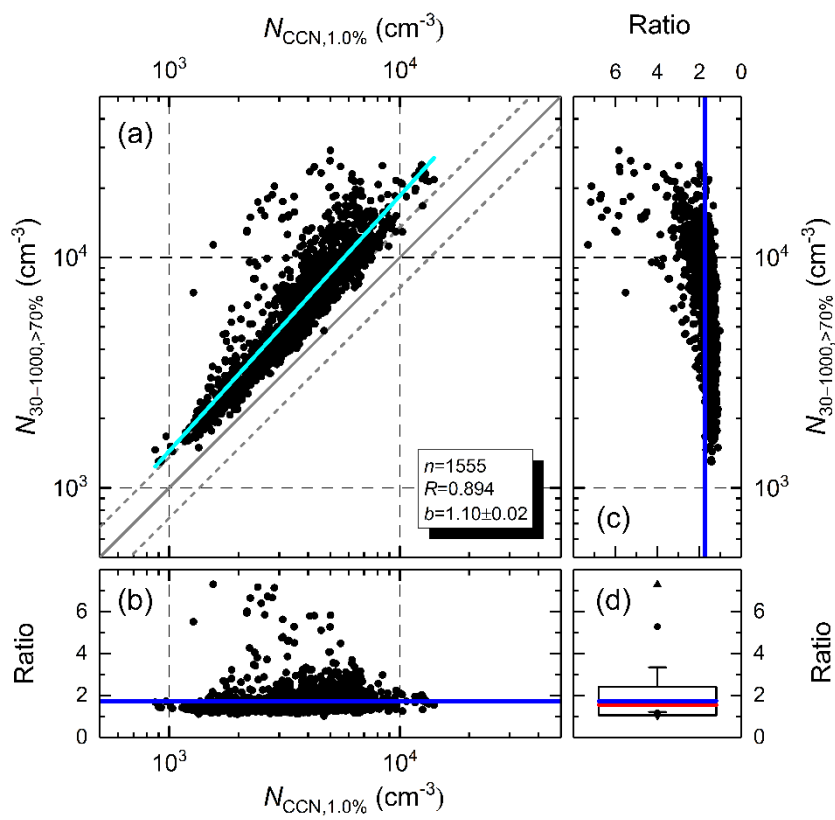
287 3.1 Data quality

288 The DMPS measured systematically smaller total particle number concentrations (N_{6-1000}) than the CPC
289 (N_{CPC}) as discussed in Sect. 2.2. The intercept (a) and slope (b) with SDs of the regression line of the
290 N_{CPC}/N_{6-1000} ratio vs. N_{6-30}/N_{6-1000} ratio were $a = 1.33 \pm 0.01$ and $b = 0.17 \pm 0.02$, respectively and the
291 Pearson's coefficient of correlation (R) between the concentration sets was 0.943. As a result of the
292 comparison, a size-independent multiplication correction factor of 1.33 was adopted for the inverted
293 DMPS data.

294

295 The scatter plot of the $N_{30-1000}$ DMPS data for which the $N_{30-1000}/N_{6-1000} > 70\%$ ($N_{30-1000, > 70\%}$; see also Sect.
296 2.2) and the $N_{CCN, 1.0\%}$ data is shown in Fig. 1a. It can be seen that all measured particle number
297 concentrations were larger than for the CCN. The $N_{30-1000, > 70\%}/N_{CCN, 1.0\%}$ ratio as function of $N_{CCN, 1.0\%}$ (Fig.
298 1b) did not indicate systematic difference between the two instruments. Most concentration ratios with
299 larger (i.e. from ca. 3 to 7) values that showed up in all panels were isolated cases from each other. They
300 were most likely related to the time difference between the actual DMPS and CCNc data. Since the
301 instruments have time resolutions of ca. 8 min and 32 min, respectively, their compared data pairs could
302 have a time difference of up to 16 min (if the first possible DMPS measured spectrum was missing).
303 During this time span, the particle number concentrations could change substantially. Actual atmospheric
304 concentrations can vary rapidly because of the changes in intensity of some important anthropogenic
305 emission sources in the vicinity, of physical removal processes and in local meteorological conditions
306 (such as WS, which influences the particle transport). The dynamic variability in concentrations often
307 happens in cities and can be witnessed as suddenly appearing stripes on the particle number size
308 distribution surface plots (e.g. Fig. 10 in Salma et al., 2016).

309
310
311
312
313
314
315
316
317
318
319
320
321
322
323
324
325
326
327



328 **Figure 1.** Relationship between the concentration of particles with a diameter >30 nm if their relative contribution to the total
329 particles was >70 % ($N_{30-1000,>70\%}$) and CCN concentration at a supersaturation of 1.0 % ($N_{CCN,1.0\%}$; a). The number of the data
330 points considered (n), their coefficient of correlation (R) and the slope (b) with SD of the regression line (in cyan) are also
331 indicated. The line of equality and the dashed grey lines indicate the range of the expected uncertainty of $\pm 15\%$ solely from
332 particle counting. The $N_{30-1000,>70\%}/N_{CCN,1.0\%}$ ratios are also shown as function of the variables $N_{CCN,1.0\%}$ (b) and $N_{30-1000,>70\%}$ (c)
333 with mean (the lines in blue colour). The box and whisker plot summarises the maximum and minimum (triangle pointing
334 upward and downward, respectively), 1st and 99th percentiles (bullets), mean with SD (blue line and the horizontal borders of
335 the box, respectively) and median (red line) of the $N_{30-1000,>70\%}/N_{CCN,1.0\%}$ ratios (d).

336

337 The $N_{30-1000,>70\%}/N_{CCN,1.0\%}$ ratio as function of $N_{30-1000,>70\%}$ (Fig. 1c) suggested that the ratio was slightly
338 increasing with the concentration, mainly above 10⁴ cm⁻³. An agreement between the $N_{30-1000,>70\%}$ and
339 $N_{CCN,1.0\%}$ is expected (approximately within $\pm 15\%$; Sect. 2.1) if the number of particles that were >30 nm
340 and that exhibited low hygroscopicity is negligible with respect to $N_{30-1000,>70\%}$. The opposite can be easily
341 realised in cities including Budapest. The argument is backed by the fact that the R between $N_{30-1000,>70\%}$
342 and N_{6-25} was significant (0.875) during the measurement year. The latter size fraction mainly contains
343 freshly emitted particles from road vehicles in most of the time (Salma et al., 2017), which typically
344 exhibit low hygroscopicity (Burkart et al., 2011; Rose et al., 2011; Enroth et al., 2018). They contribute
345 to the $N_{30-1000,>70\%}$ as well. Another indication of the chemical species with low hygroscopicity is the low
346 contribution of water-soluble organic carbon (WSOC) and high contribution of elemental carbon (soot)
347 to organic carbon (OC), which are roughly related to general hygroscopicity, in central Budapest. The
348 former ratio was substantially lower (WSOC/OC ratios from 20 to 39 %), while the latter ratio was

349 considerably larger (EC/OC ratios from 14 to 20 %) in comparison with the aerosol that was already
 350 chemically aged or can be found above regional or remote areas (Salma et al., 2007, 2020a and references
 351 therein).

352
 353 All this implies that the importance of the average $N_{30-1000,>70\%}/N_{CCN,1.0\%}$ ratio has to be extended or even
 354 preceded by the slope of the regression line and R of the two data sets as suggestive metrics for quality
 355 assurance. The mean ratio with SD and median ratio of $N_{30-1000,>70\%}/N_{CCN,1.0\%}$; the slope of the regression
 356 line with SD; and the coefficient of correlation for the overall data set were 1.73 ± 0.67 , 1.56, 1.10 ± 0.02
 357 and 0.894, respectively. Our set of quality indicators fits into the results of the data quality check
 358 elaborated for a number of other, mainly regional locations (Schmale et al., 2017). They jointly suggest
 359 that the CCNc and DMPS instruments were operating in a coherent manner and that the CCNc instrument
 360 performed reasonably well over the whole measurement year.

361 3.2 Concentrations and their ratios

362 The basic statistical measures of the particle number concentrations in different size fractions over the
 363 whole measurement year are summarised in Table 1. The mean ratio and SD of N_{6-100}/N_{6-1000} were
 364 (81 ± 10) %. The concentrations are comparable with but somewhat larger than our earlier annual results,
 365 while the ratios agree well with the previous data (Mikkonen et al., 2020). The median particle number
 366 size distribution is shown in Fig. S1.

367
 368 **Table 1.** Ranges, medians and means with SDs of the particle number concentrations in the diameter ranges from 6 to 25 nm
 369 (N_{6-25}), from 6 to 100 nm (N_{6-100}), from 30 to 1000 nm ($N_{30-1000}$), from 30 to 1000 nm if their contribution to total particles was
 370 >70 % ($N_{30-1000,>70\%}$) and from 6 to 1000 nm (N_{6-1000}) in a unit of 10^3 cm^{-3} .

Statistics	N_{6-25}	N_{6-100}	$N_{30-1000}$	$N_{30-1000,>70\%}$	N_{6-1000}
Min	0.069	0.66	0.26	0.81	0.76
Median	4.0	8.2	4.9	6.0	10.1
Max	137	153	47	39	154
Mean	5.3	10.1	6.0	7.2	12.1
SD	5.1	7.4	3.9	4.6	8.1

372
 373 It is noted for completeness that the median N_{6-100} and N_{6-1000} during the restriction on movements of the
 374 first outbreak of the COVID-19 pandemic were smaller than the annual median levels by 72 and 79 %,
 375 respectively, while the $N_{30-1000}$ remained similar. The mean N_{6-100}/N_{6-1000} and SD of (75 ± 12) % indicated
 376 that the share of the ultrafine particles substantially decreased (cf. the previous paragraph). All this is in
 377 accordance with the conclusions of our more extensive study dedicated to this issue (Salma et al., 2020b).

378

379 The basic statistical measures of the CCN concentrations at different S s over the whole measurement year
380 are surveyed in Table 2. It is mentioned for completeness that some individual CCN concentrations at S s
381 of 0.5 and 1.0 % were above $9 \times 10^3 \text{ cm}^{-3}$ (Sect. 1), but only in 10 (0.073 % of all relevant data) and 59
382 cases (0.43 %), respectively, whereas the related κ values were rather low (Sect. 3.5). Therefore, the CCN-
383 limited regime of droplet activation was realised. The median concentration changed monotonically from
384 0.59×10^3 to $2.5 \times 10^3 \text{ cm}^{-3}$ with S and showed a levelling off tendency. They were fitted by a power law
385 function in the form of $N_{\text{CCN},S} = c \times S^k$, where S is the supersaturation in % (in Origin Pro 2017 software
386 using the Levenberg–Marquardt iteration algorithm) to obtain the so-called traditional CCN spectrum
387 (Pruppacher and Klett, 2000). The constant c corresponds to the CCN concentration at an S of 1.0 %. The
388 knowledge of these 2 parameters is sufficient for some cloud microphysics applications. The fitted
389 parameters c and k with SDs obtained were $(2.81 \pm 0.12) \times 10^3 \text{ cm}^{-3}$ and 0.52 ± 0.05 , respectively. The
390 coefficient c agreed with the measured average $N_{\text{CCN},1.0\%}$ (Table 2). The exponent k was within the interval
391 reported for other continental locations ($k=0.4\text{--}0.9$; Pruppacher and Klett, 2000). The fitted function
392 reproduced the experimental data at higher (>0.2 %) S s satisfactorily, while their ratio became 1.25 at an
393 S of 0.1 %. The comparison of the concentrations with other locations is accomplished together with the
394 effective critical dry particle diameters in Sect. 3.3.

395

396 **Table 2.** Ranges, medians and means with SDs of the CCN concentrations (in $\times 10^3 \text{ cm}^{-3}$) at supersaturations of 0.1, 0.2, 0.3,
397 0.5 and 1.0 %.

398

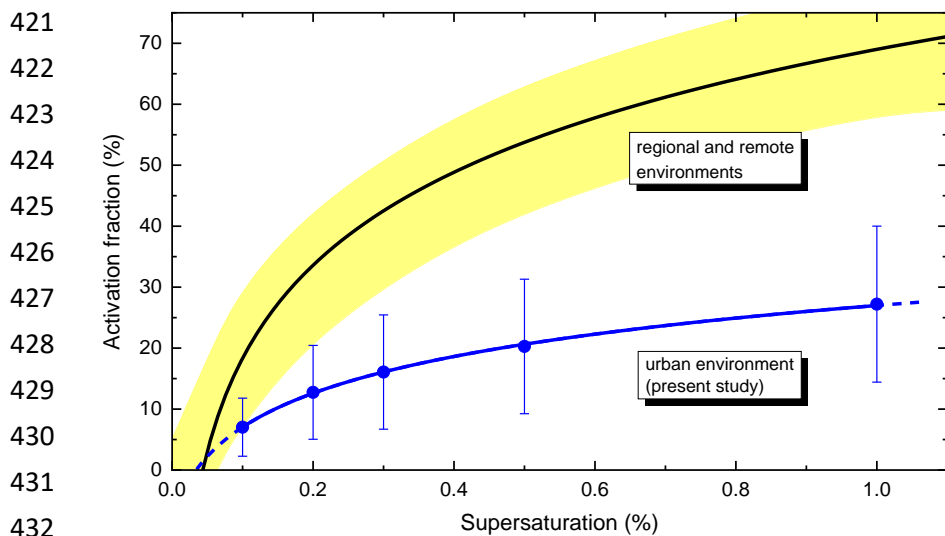
Statistics	0.1 %	0.2 %	0.3 %	0.5 %	1.0 %
Min	0.025	0.076	0.100	0.108	0.143
Median	0.59	1.09	1.39	1.80	2.5
Max	2.9	5.6	8.1	10.1	14.1
Mean	0.67	1.25	1.59	2.0	2.7
SD	0.41	0.74	0.97	1.2	1.5

399

400 The mean activation fractions ($\text{AF} = N_{\text{CCN},S} / N_{6-1000}$) of the particles increased monotonically from 7 to 27
401 % with S and indicated some levelling off character (Fig. 2). The activation curve was obtained by fitting
402 the experimental data with a two-parameter logarithm function of $\text{AF} = a \times \ln(S) + b$, where a and b are the
403 fitting parameters (Paramonov et al., 2015) in Origin Pro 2017 software using the Levenberg–Marquardt
404 iteration algorithm. Its shape was similar to that for the CCN concentrations. This is typical for non-
405 coastal locations, where a multicomponent mixture of particle sources yield more-or-less balanced and,
406 therefore, similar curves (Schmale et al., 2018). Figure 2 also contains the annual activation curve
407 obtained in a synthesis study of the European Aerosol Cloud Climate and Air Quality Interactions project
408 by fitting the mean AFs for several regional and remote locations with an identical function (Fig. 5 in
409 Paramonov et al., 2015). It can be seen that the curves for the urban and the other sites were rather different

410 from each other in magnitudes or placement. The urban AFs were very substantially and systematically
 411 smaller than for the regional and remote locations. This was also witnessed with regard to other regional
 412 results (Sihto et al, 2011), and could be an urban feature. The low AF in cities can likely be explained by
 413 larger particle number concentrations, higher abundance of small particles that do not activate and by a
 414 chemical composition that can be characterised with typically lower hygroscopicity than for regional
 415 aerosol. At the same time, the relative SDs (RSDs) of our mean values were relatively high (between 45
 416 and 70 %), which pointed to a considerable time variability of both N_{6-1000} and $N_{CCN,S}$. It also hinted that
 417 the prediction of CCN concentrations based solely on particle number concentrations and mean AFs are
 418 expected not to be reliable in urban environments. Moreover, the annual curves do not necessary capture
 419 the variability on shorter or seasonal scales.

420



433 **Figure 2.** Mean activated fractions of total particles (N_{6-1000}) with SDs derived for central Budapest at supersaturations of 0.1,
 434 0.2, 0.3, 0.5 and 1.0 % (experimental data in blue) together with their fitted dependency (line in blue). The fitting function was
 435 $AF=a \times \ln(S)+b$, with parameters of $a=34.8 \pm 0.4$ and $b=26.7 \pm 0.3$. The line in black is shown for comparative purposes and was
 436 calculated by an identical function with the mean parameters of $a=22$ and $b=69$ that were obtained for several selected regional
 437 and remote sites in a EUCAARI synthesis study (Table 4; Paramonov et al., 2015). The yellow band represents the 95 %
 438 confidence interval.

439 3.3 Effective critical dry particle diameters

440 Basic statistical measures of the effective critical dry particle diameters at different S_s over the whole
 441 measurement year are displayed in Table 3. The median $d_{c,eff}$ decreased from 207 to 80 nm with S . All
 442 diameters were positioned within the accumulation mode of the median particle number size distribution
 443 (Fig. S1). The monthly mean number median mobility diameters for the Aitken and accumulation modes
 444 were typically 26 and 93 nm, respectively with an identical geometric SDs (GSDs) of 2.1 (Salma et al.,
 445 2011). The broadening was caused by averaging the individual size distributions. Considering the
 446 minimum of the $d_{c,eff}$ data, some individual diameters, in particular for S_s of 0.5 and 1.0 %, could be
 447 shifted to the Aitken mode.

448

449 **Table 3.** Ranges, medians and means with SDs of the effective critical dry particle diameters in units of nm at supersaturations
 450 of 0.1, 0.2, 0.3, 0.5 and 1.0 %.

451

Statistics	0.1 %	0.2 %	0.3 %	0.5 %	1.0 %
Min	134	92	74	56	38
Median	207	149	126	105	80
Max	455	320	271	225	173
Mean	213	153	130	109	83
SD	32	26	24	22	20

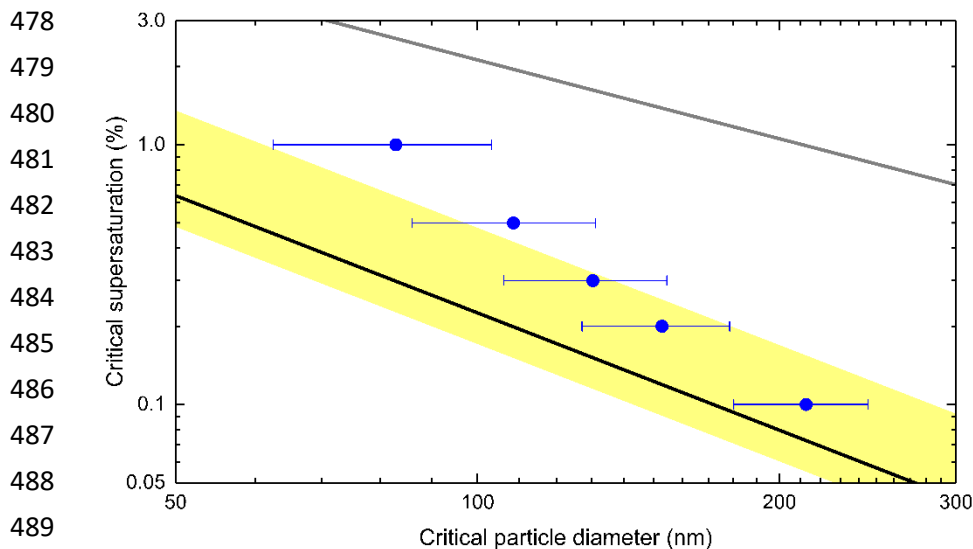
452

453 The present average diameters and CCN concentrations were larger than for coastal or rural background,
 454 forested or remote environments (Henning et al., 2002; Komppula et al., 2005; Paramonov et al., 2015;
 455 Schmale et al., 2018). This confirmed that the water activation properties depend on the aerosol type. Our
 456 data were comparable with other urban sites (Kuwata and Kondo, 2008; Rose et al., 2010; Burkart et al.,
 457 2011; Meng et al., 2014). The modifications within the location category can likely be associated with
 458 relatively large differences between urban aerosol properties. The mean contribution and SD of ultrafine
 459 particles were, for instance, $N_{6-100}/N_{6-1000}=(81\pm 10)$ % in Budapest and $N_{13-100}/N_{13-929}=75$ % in Vienna.
 460 The present $d_{c,eff}$ data were also contrasted with the computed results for the simulated global continental
 461 mean κ value and SD of 0.27 ± 0.21 (Pringle et al., 2010) in Fig. 3. The lines were obtained using the
 462 parameters given in Sect. 2.3. The data points belong to different parallel lines with a theoretical slope of
 463 $-3/2$. They suggested that the urban aerosol particles in Budapest with a diameter larger than
 464 approximately 130 nm showed similar hygroscopicity to continental aerosol in general, whereas the
 465 smaller particles appeared to be less hygroscopic. The distinctions were even larger when European
 466 continental aerosol is considered ($\kappa=0.36$; Pringle et al., 2010). The data points fairly tended toward the
 467 limiting relationship for insoluble but wettable particles by decreasing diameter. Freshly emitted soot
 468 particles could be an example of them (Rose et al., 2011).

469

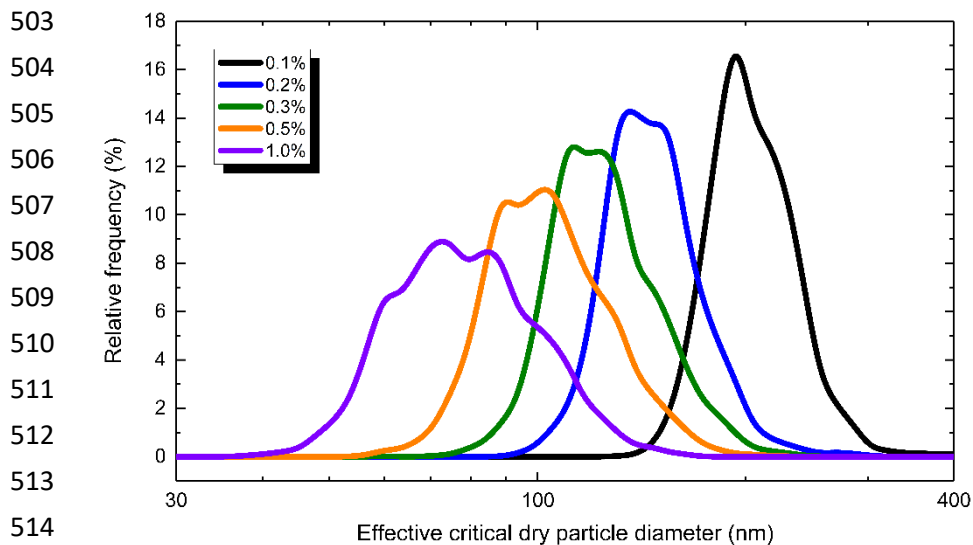
470 The tendentious dependency of the deviation of the experimentally derived ($d_{c,eff}$, S_c) data points from the
 471 line for the simulated global continental mean κ (Fig. 3) also pointed to the size-dependent chemical
 472 composition, which is likely more pronounced for urban particles. All this is in line with the ideas on the
 473 major source types such as vehicle emissions, biomass burning or new particle formation and diameter
 474 growth (NPF) events (Salma et al., 2014, 2017, 2020a, 2020b) and the particle number size distributions
 475 in Budapest (Salma et al., 2011). Photochemical processing may also play a role through chemical ageing
 476 (Furutani et al., 2008). As a result, the urban sources often result in external mixtures of particles.

477



478
 479
 480
 481
 482
 483
 484
 485
 486
 487
 488
 489
 490 **Figure 3.** Critical supersaturation and effective critical dry particle diameter data pairs with SDs (in blue) determined
 491 experimentally in central Budapest and the dependency calculated for the simulated global continental mean κ and SD of
 492 0.27 ± 0.21 . The line in black was obtained for the mean κ value and the yellow band represents ± 1 SD. The relationship for
 493 insoluble but wettable particles ($\kappa=0$, the Kelvin term) was displayed by the line in grey for comparative purposes.

494
 495 Frequency distributions of $d_{c,eff}$ at an S can be described by a lognormal distribution function. The
 496 normalised differential distributions of the $d_{c,eff}$ data for each S are shown in Fig. 4. They were derived
 497 by partitioning all diameter data into 71 intervals with an equal width of 0.0243 on logarithmic scale
 498 between 10 and 500 nm. The selections proved to be a reasonable compromise between the good statistics
 499 and good data resolution. The distributions exhibited single peaks with geometric SDs increasing
 500 monotonically with S as 1.14, 1.16, 1.20, 1.22 and 1.27, respectively. The broadening indicated larger
 501 variability in droplet activation properties of the smaller particles.



502
 503
 504
 505
 506
 507
 508
 509
 510
 511
 512
 513
 514
 515 **Figure 4.** Differential frequency distributions of effective critical dry particle diameters at supersaturations of 0.1, 0.2, 0.3, 0.5
 516 and 1.0 % normalised to the total counts of the diameter data.

517

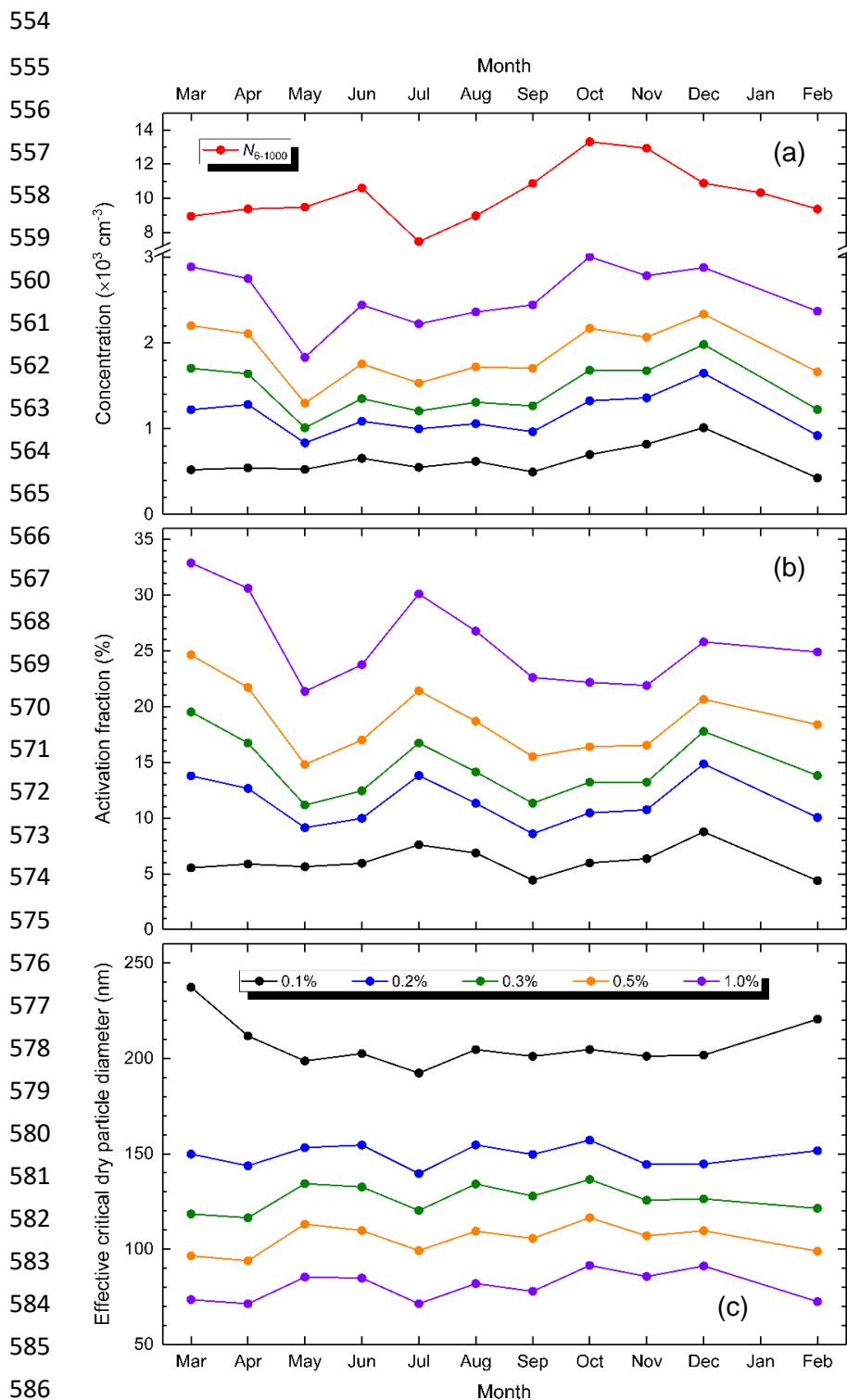
518 The peaks exhibited a fine structure. They seemed to contain submodes. This is likely related to the
519 mixtures of particles with different activation properties. The submodes could be produced by sources
520 which result in particles with different chemical composition and mixing states. These differences may
521 not necessarily show up in the particle number size distributions, while they can lead to diverse activation
522 properties. Several compositional elements of the fine structure (e.g. the maximum or the relative peak
523 areas) changed in a tendentious manner by S . Their exact identification and interpretation are beyond the
524 objectives of the present paper. They are to be included into an upcoming study which is to deal with the
525 relationships of major source types such as vehicle emissions, NPF events or biomass burning and the
526 activation properties of CCN together with their diurnal variability and air mass trajectories.

527 **3.4 Seasonal cycling**

528 The time series of the experimental data showed high variability in time. The monthly medians seemed
529 to be more advantageous for investigating the possible seasonal cycling (Fig. 5). It is noted that medians
530 were selected as characteristics instead of means and SDs since these probability variables can be
531 described by lognormal distribution functions (Sect. 3.2). The months were organised to represent the
532 spring (MAM), summer (JJA), autumn (SON) and winter (DJF) seasons. Stricter chronological ordering
533 of the months seems to be more advantageous for source-related or dynamic studies on various timescales.

534
535 The dependencies for the separate variables were similar to each other at different S s. The changes were
536 pronounced mainly for the larger S s, which are the least relevant for an ambient air. This already indicates
537 that the seasonal cycling does not very likely or substantially influence the aerosol–water vapour
538 interactions under ordinary environmental conditions. The CCN concentrations appeared somewhat
539 smaller from May to September, and somewhat larger in the other months. Their minimum was typically
540 in May. These intervals coincided with the non-heating (formally from 15 April to 15 October) and
541 heating seasons (the rest of the year) in Hungary. As an exception, the concentrations for February were
542 unusually small. The AFs appeared to be smaller in May (and perhaps also in June) and September (and
543 perhaps also in October), and larger in the other months. The comparison of the monthly median $N_{CCN,S}$
544 and AF to the dependency of the total particle numbers implied that the seasonal variations of the former
545 two properties were not mainly due to the variations in the particle number concentrations. No obvious
546 dependency for the monthly median $d_{c,eff}$ values could be established since their distributions were
547 featureless. The lack of cycling meant that the particles in Budapest exhibited more or less similar droplet
548 activation behaviour over the year. This was different from some other, non-urban locations (Pringle et
549 al., 2010; Sihto et al., 2011; Paramonov et al., 2013, 2015; Schmale et al., 2018). It is also noted that the
550 $d_{c,eff}$ values for an S of 0.1 % were segregated somewhat more from the other dependencies. It has to be
551 added that March and April 2020 were extraordinary due to the first outbreak of the COVID-19 pandemic

552 in Hungary. Firmer seasonal dependencies require longer measurements since the related properties can
 553 also be influenced by inter-annual variability.



587 **Figure 5.** Time series of the monthly median CCN concentrations and total particle number concentration (N_{6-1000} ; a),
 588 activation fractions (b) and effective critical dry particle diameters (c) at supersaturations of 0.1, 0.2, 0.3, 0.5 and 1.0 %.

589
 590 Supersaturations of ca. 0.1 % ordinarily occur in warm stratiform clouds, and these Ss activate only larger
 591 ($d > 200 \text{ nm}$) particles. Chemical composition of these particles are usually more balanced over the year
 592 than for smaller particles due to, for instance, chemical and physical ageing and particle mixing processes.

593 Therefore, it can be concluded that differences in chemical composition do not seem to play a crucial role
594 in cloud activation properties even in cities.

595 **3.5 Hygroscopicity parameters**

596 The basic statistical measures of the κ values for different S s over the whole measurement year are given
597 in Table 4. All characteristics decreased monotonically and showed a levelling off tendency with S . The
598 averages implied in general that the larger particles exhibited higher hygroscopicity than the smaller
599 particles. When considering also the $d_{c,eff}$ data which belong to the S s, the present hygroscopicity
600 parameters fairly agreed with the values derived previously from volatility and hygroscopicity tandem
601 differential mobility analyser (VH-TDMA) measurements under subsaturated conditions (RH=90 %) at
602 the identical site (Enroth et al., 2018). In that study, the nearly hydrophobic particles exhibited a mean κ
603 value of 0.033. The mode typically contained 69 % of particles at a dry diameter of 50 nm, and the κ
604 seemed to be independent of the particle diameter in the range from 50 to 145 nm. The less hygroscopic
605 particles showed larger mean κ value of 0.20. They typically made up 59 % of particles at 145 nm.

606

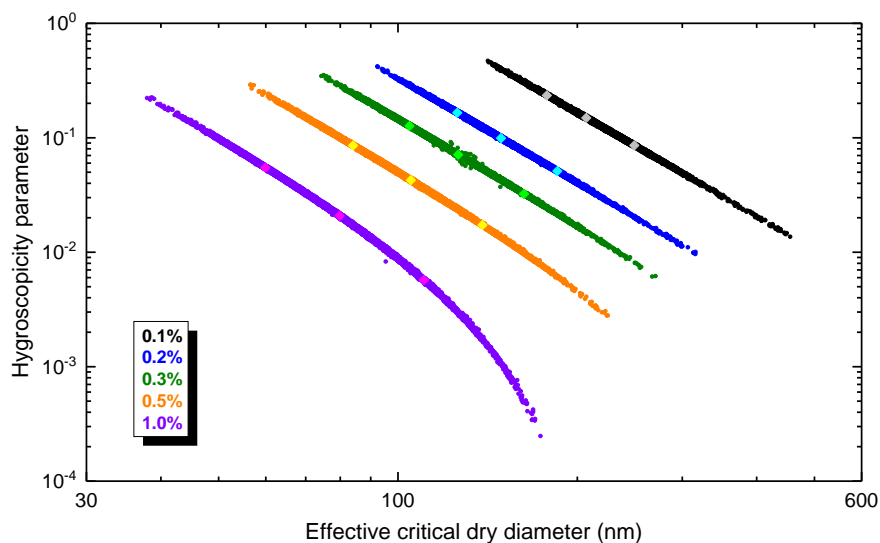
607 The range of the κ values was increasing with S , and, more importantly, it became particularly large (a
608 factor of ca. 10^3 for 1.0 %) even when compared with aerosol properties typically driven by atmospheric
609 dynamics. This can be illustrated by the relationships between the κ value and $d_{c,eff}$ for each S (Fig. 6).
610 The data sets created separate lines or narrow stripes with a theoretical slope of -3 over the main range
611 of the variables considered assuming that the other physicochemical properties such as d_{wet} , T_a , $\sigma_{d/a}$ and
612 ρ_w do not change substantially. The line for the S of 1.0 % was bended at low κ and large $d_{c,eff}$. This is
613 also in accordance with the κ -Köhler model (Eq. 2). It can be seen that the data pairs shown for a given
614 S level indeed cover a wide interval of the related variables. Such variability in κ did not back the idea of
615 using just a single characteristic value for a given S , and an effective κ parameter or its function on particle
616 size would be preferred instead (Paramonov et al., 2015). The average hygroscopicity parameter
617 represented the particles with a size close to the effective critical dry particle diameter. Furthermore, the
618 distributions of the data pairs along the lines were not completely symmetric with respect to the medians,
619 which confirmed the fine structure of the frequency distributions (Sect. 3.3). The 3 characteristic points
620 (10th, 50th and 90th percentiles) on the lines indicated a broadening of the frequency distributions with S .
621 The frequency distribution of the hygroscopicity parameters in 71 intervals with an equal width of 0.0571
622 on logarithmic scale between 10^{-4} and 10^0 are shown in Fig. S2. They largely reflect the behaviour and
623 tendencies of the effective critical dry particle diameter (Fig. 4) since their computations involved $d_{c,eff}$.

624

625 **Table 4.** Ranges, medians and means with SDs for the hygroscopicity parameter at supersaturations of 0.1, 0.2, 0.3, 0.5 and
 626 1.0 %.

Statistics	0.1 %	0.2 %	0.3 %	0.5 %	1.0 %
Min	0.014	0.010	0.006	0.003	0.0003
Median	0.149	0.099	0.071	0.043	0.021
Max	0.47	0.42	0.35	0.29	0.22
Mean	0.154	0.106	0.078	0.049	0.027
SD	0.061	0.048	0.041	0.031	0.022

628
 629 The average κ values were considerably smaller than for regional or remote locations (Paramonov et al.,
 630 2015; Schmale et al., 2018). There are few hygroscopicity parameters reported specifically for urban
 631 environments, and even less for city centres (Gunthe et al., 2011; Rose et al., 2010, 2011; Meng et al.,
 632 2014; Arub et al., 2020). The present data can also be linked to the average or effective hygroscopicity
 633 parameters found in field measurements and chamber studies for fresh soot particles of <0.01 , for
 634 secondary organic aerosol of approximately 0.10 and for inorganic aerosol fraction of ca. 0.64 (Rose et
 635 al., 2011). All this pointed to the presence of freshly emitted and externally mixed soot particles with very
 636 low hygroscopicity in high abundancies in central Budapest.



637
 638
 639
 640
 641
 642
 643
 644
 645
 646
 647
 648
 649
 650 **Figure 6.** Relationship of the hygroscopicity parameter and the effective critical dry particle diameter ($d_{c,eff}$) derived at
 651 supersaturations of 0.1, 0.2, 0.3, 0.5 and 1.0 %. The three diamond symbols in lighter colours on each data set represent the
 652 data pairs belonging to the 10th and 90th percentiles; 50th and 50th percentiles; and 90th and 10th percentiles in the order of
 653 increasing $d_{c,eff}$.

654 4 Conclusions

655 Concentrations of CCN at various S_s and particle number size distributions were measured in parallel
 656 with each other in a continental central European urban environment over 1 year. The effective cloud

657 droplet activation properties of the aerosol population were determined from the available experimental
658 data without measuring the time-resolved chemical composition. The results indicated several urban
659 specialities. The average CCN concentrations were substantially larger, whereas the average effective
660 critical dry particle diameters and activation fractions were considerably and systematically smaller than
661 for non-urban sites. The particles with a diameter of ca. 130 nm already showed lower hygroscopicity
662 than in general, and the difference between the urban and general hygroscopic properties was further
663 enhanced for decreasing size. These urban features can likely be related to the high abundance of freshly
664 emitted less-hygroscopic particles including soot and to substantial differences in the size-dependent
665 chemical composition and mixing states of particles in cities. The seasonal dependencies in N_{CCN} and
666 activation fractions at various S s were only loosely connected to the total particle number concentrations.
667 The achieved results represent the first information of this type for a city in the Carpathian Basin and
668 contribute to our general knowledge on and understanding of urban atmospheric environments.

669

670 The measurements were performed at a fix location in central Budapest, which can be regarded as an
671 urban background site. The obtained results and conclusions are representative for the average or overall
672 atmosphere of the city centre. Some urban microenvironments such as kerbside sites, street canyons, road
673 junctions or suburban areas exhibit diverse size distributions and chemical composition, and, therefore,
674 certain differences in hygroscopic properties are expected among them. Furthermore, some relevant
675 meteorological conditions can also change within the urban canopy due to, for instance, heat islands often
676 realised in large cities. At the same time, the related atmospheric processes likely occur on larger spatial
677 scales than the city itself or its central part. From this point of view, the data derived for the urban
678 background appear to be a sensible starting approximation to reality. Further dedicated studies preferably
679 involving surface measurements, satellite products and modelling can contribute to an understanding of
680 the challenging issue of the urban climate.

681

682 The water uptake properties of urban aerosol particles under both sub- and supersaturation conditions are
683 increasingly recognised also because of their relevance in urban climate considerations and in particle
684 deposition modelling in the human respiratory system. The κ values determined here are to be further
685 utilised in health-related studies as well.

686

687 After gaining experience with operation and calibration of the dual-chamber CCNc measurement system,
688 we plan to extend one of its chambers by a DMA and CPC setup so we can perform both polydisperse
689 and monodisperse measurements in parallel, which is expected to supply further valuable knowledge on
690 the mixing states of particles. This is especially important since urban aerosol particles typically comprise
691 externally mixed carbonaceous particles with very distinct hygroscopic properties. This seems to be

692 relevant in general and could also support or facilitate the association of the hygroscopicity parameters to
693 major source types in cities together with multistatistical apportionment methods.

694 *Data availability.* The observational data are available from the corresponding author.

695 *Supplement.* The supplement related to this article is available online:

696 *Author contributions.* IS conceived, designed and lead the research; WT and AZGy performed the measurements; MV
697 developed the ASL data evaluation software; IS, MV and WT accomplished the data treatment and prepared the figures; IS,
698 WT, MV and AZGy interpreted the results; IS wrote the manuscript with comments from all coauthors.

699 *Competing interests.* The authors declare that they have no conflict of interest.

700 *Financial support.* This research has been supported by the Hungarian Research, Development and Innovation Office (grant
701 no. K132254) and by the European Regional Development Fund and the Hungarian Government (GINOP-2.3.2-15-2016-
702 00028).

703 **References**

- 704 Andreae, M. O. and Rosenfeld, D.: Aerosol-cloud-precipitation interactions. Part 1. The nature and sources of cloud-active
705 aerosols, *Earth Sci. Rev.*, 89, 13–41, <https://doi.org/10.1016/j.earscirev.2008.03.001>, 2008.
- 706 Andreae, M. O., Jones, C. D., and Cox, P. M.: Strong present-day aerosol cooling implies a hot future, *Nature*, 435, 1187–
707 1190, <https://doi.org/10.1038/nature03671>, 2005.
- 708 Arub, Z., Bhandari, S., Gani, S., Apte, J. S., Hildebrandt Ruiz, L., and Habib, G.: Air mass physiochemical characteristics
709 over New Delhi: impacts on aerosol hygroscopicity and cloud condensation nuclei (CCN) formation, *Atmos. Chem.*
710 *Phys.*, 20, 6953–6971, <https://doi.org/10.5194/acp-20-6953-2020>, 2020
- 711 Burkart, J., Steiner, G., Reischl, G., and Hitzenberger, R.: Longterm study of cloud condensation nuclei (CCN) activation of
712 the atmospheric aerosol in Vienna, *Atmos. Environ.*, 45, 5751–5759, <https://doi.org/10.1016/j.atmosenv.2011.07.022>,
713 2011.
- 714 Carslaw, K., Lee, L., Reddington, C., Pringle, K., Rap, A., Forster, P., Mann, G., Spracklen, D., Woodhouse, M., and
715 Regayre, L.: Large contribution of natural aerosols to uncertainty in indirect forcing, *Nature*, 503, 67–71,
716 <https://doi.org/10.1038/nature12674>, 2013.
- 717 Dusek, U., Frank, G. P., Hildebrandt, L., Curtius, J., Schneider, J., Walter, S., Chand, D., Drewnick, F., Hings, S., Jung, D.,
718 Bormann, S., and Andreae, M. O.: Size matters more than chemistry for cloud-nucleating ability of aerosol particles,
719 *Science*, 312, 1375–1378, <https://doi.org/10.1126/science.1125261>, 2006.
- 720 Enroth, J., Mikkilä, J., Németh, Z., Kulmala, M., and Salma, I.: Wintertime hygroscopicity and volatility of ambient urban
721 aerosol particles, *Atmos. Chem. Phys.*, 18, 4533–4548, <https://doi.org/10.5194/acp-18-4533-2018>, 2018.
- 722 Facchini, M. C., Mircea, M., Fuzzi, S., and Charlson, R. J.: Cloud albedo enhancement by surface-active organic solutes in
723 growing droplets, *Nature*, 401, 257–259, <https://doi.org/10.1038/45758>, 1999.
- 724 Furutani, H., Dall'osto, M., Roberts, G. C., and Prather, K. A.: Assessment of the relative importance of atmospheric aging
725 on CCN activity derived from measurements, *Atmos. Environ.*, 42, 3130–3142,
726 <https://doi.org/10.1016/j.atmosenv.2007.09.024>, 2008.
- 727 Gunthe, S. S., Rose, D., Su, H., Garland, R. M., Achtert, P., Nowak, A., Wiedensohler, A., Kuwata, M., Takegawa, N.,
728 Kondo, Y., Hu, M., Shao, M., Zhu, T., Andreae, M. O., and Pöschl, U.: Cloud condensation nuclei (CCN) from fresh and
729 aged air pollution in the megacity region of Beijing, *Atmos. Chem. Phys.*, 11, 11023–11039, <https://doi.org/10.5194/acp-11-11023-2011>, 2011.
- 731 Gysel, M. and Stratmann, F.: WP3 – NA3: In-situ chemical, physical and optical properties of aerosols, Deliverable D3.11:
732 Standardized protocol for CCN measurements, Tech. rep., available at: [https://studylib.net/doc/18744398/standardized-
733 protocol-for-long-term-cloud-condensation](https://studylib.net/doc/18744398/standardized-protocol-for-long-term-cloud-condensation) (last access: 2 April 2021), 2013.
- 734 Henning, S., Weingartner, E., Schmidt, S., Weindisch, M., Gäggeler, H. W., and Baltensperger, U.: Size-dependent aerosol
735 activation at the high-alpine site Jungfraujoch (3580m a.s.l.), *Tellus B*, 54, 82–95,
736 <https://doi.org/10.3402/tellusb.v54i1.16650>, 2002.
- 737 Herenz, P., Wex, H., Henning, S., Kristensen, T. B., Rubach, F., Roth, A., Borrmann, S., Bozem, H., Schulz, H., and
738 Stratmann, F.: Measurements of aerosol and CCN properties in the Mackenzie River delta (Canadian Arctic) during
739 spring–summer transition in May 2014, *Atmos. Chem. Phys.*, 18, 4477–4496, <https://doi.org/10.5194/acp-18-4477-2018>,
740 2018.
- 741 Hudson, J.: Variability of the relationship between particle size and cloud nucleating ability, *Geophys. Res. Lett.*, 34, L08801,
742 <https://doi.org/10.1029/2006GL028850>, 2007.
- 743 Jurányi, Z., Gysel, M., Weingartner, E., DeCarlo, P. F., Kammermann, L., and Baltensperger, U.: Measured and modelled
744 cloud condensation nuclei number concentration at the high alpine site Jungfraujoch, *Atmos. Chem. Phys.*, 10, 7891–
745 7906, <https://doi.org/10.5194/acp-10-7891-2010>, 2010.

746 Jurányi, Z., Gysel, M., Weingartner, E., Bukowiecki, N., Kammermann, L., and Baltensperger, U.: A 17 month climatology
747 of the cloud condensation nuclei number concentration at the high alpine site Jungfraujoch, *J. Geophys. Res.-Atmos.*,
748 116, D10204, <https://doi.org/10.1029/2010JD015199>, 2011.

749 Kammermann, L., Gysel, M., Weingartner, E., Herich, H., Cziczó, D. J., Holst, T., Svenningsson, B., Arneth, A., and
750 Baltensperger, U.: Subarctic atmospheric aerosol composition: 3. Measured and modeled properties of cloud
751 condensation nuclei, *J. Geophys. Res.*, 115, 04202, <https://doi.org/10.1029/2009JD012447>, 2010.

752 Kerminen, V.-M., Paramonov, M., Anttila, T., Riipinen, I., Fountoukis, C., Korhonen, H., Asmi, E., Laakso, L., Lihavainen,
753 H., Swietlicki, E., Svenningsson, B., Asmi, A., Pandis, S. N., Kulmala, M., and Petäjä, T.: Cloud condensation nuclei
754 production associated with atmospheric nucleation: a synthesis based on existing literature and new results, *Atmos.*
755 *Chem. Phys.*, 12, 12037–12059, <https://doi.org/10.5194/acp-12-12037-2012>, 2012.

756 Komppula, M., Lihavainen, H., Kerminen, V.-M., Kulmala, M., and Viisanen, Y.: Measurements of cloud droplet activation
757 of aerosol particle at a clean subarctic background site, *J. Geophys. Res.*, 110, 06204,
758 <https://doi.org/10.1029/2004JD005200>, 2005.

759 Kuwata, M. and Kondo Y.: Dependence of size-resolved CCN spectra on the mixing state of nonvolatile cores observed in
760 Tokyo, *J. Geophys. Res.*, 113, 19202, <https://doi.org/10.1029/2007JD009761>, 2008.

761 McFiggans, G., Artaxo, P., Baltensperger, U., Coe, H., Facchini, M.-C., Feingold, G., Fuzzi, S., Gysel, M., Laaksonen, A.,
762 Lohmann, U., Mentel, T. F., Murphy, D. M., O'Dowd, C. D., Snider, J. R., and Weingartner, E.: The effect of physical
763 and chemical aerosol properties on warm cloud droplet activation, *Atmos. Chem. Phys.*, 6, 2593–2649,
764 <https://doi.org/10.5194/acp-6-2593-2006>, 2006.

765 Merikanto, J., Spracklen, D. V., Mann, G. W., Pickering, S. J., and Carslaw, K. S.: Impact of nucleation on global CCN,
766 *Atmos. Chem. Phys.*, 9, 8601–8616, <https://doi.org/10.5194/acp-9-8601-2009>, 2009.

767 Mikkonen, S., Németh, Z., Varga, V., Weidinger, T., Leinonen, V., Yli-Juuti, T., and Salma, I.: Decennial time trends and
768 diurnal patterns of particle number concentrations in a central European city between 2008 and 2018, *Atmos. Chem.*
769 *Phys.*, 20, 12247–12263, <https://doi.org/10.5194/acp-20-12247-2020>, 2020.

770 Meng, J. W., Yeung, M. C., Li, Y. J., Lee, B. Y. L., and Chan, C. K.: Size-resolved cloud condensation nuclei (CCN)
771 activity and closure analysis at the HKUST Supersite in Hong Kong, *Atmos. Chem. Phys.*, 14, 10267–10282,
772 <https://doi.org/10.5194/acp-14-10267-2014>, 2014.

773 Ovadnevaite, J., Zuend, A., Laaksonen, A., Sanchez, K. J., Roberts, G., Ceburnis, D., Decesari, S., Rinaldi, M., Hodas, N.,
774 Facchini, M. C., Seinfeld, J. H., and O'Dowd, C.: Surface tension prevails over solute effect in organic-influenced cloud
775 droplet activation, *Nature*, 546, 637–641, <https://doi.org/10.1038/nature22806>, 2017.

776 Paramonov, M., Aalto, P. P., Asmi, A., Prisle, N., Kerminen, V.-M., Kulmala, M., and Petäjä, T.: The analysis of size-
777 segregated cloud condensation nuclei counter (CCNC) data and its implications for cloud droplet activation, *Atmos.*
778 *Chem. Phys.*, 13, 10285–10301, <https://doi.org/10.5194/acp-13-10285-2013>, 2013.

779 Paramonov, M., Kerminen, V.-M., Gysel, M., Aalto, P. P., Andreae, M. O., Asmi, E., Baltensperger, U., Bougiatioti, A.,
780 Brus, D., Frank, G. P., Good, N., Gunthe, S. S., Hao, L., Irwin, M., Jaatinen, A., Jurányi, Z., King, S. M., Kortelainen, A.,
781 Kristensson, A., Lihavainen, H., Kulmala, M., Lohmann, U., Martin, S. T., McFiggans, G., Mihalopoulos, N., Nenes, A.,
782 O'Dowd, C. D., Ovadnevaite, J., Petäjä, T., Pöschl, U., Roberts, G. C., Rose, D., Svenningsson, B., Swietlicki, E.,
783 Weingartner, E., Whitehead, J., Wiedensohler, A., Wittbom, C., and Sierau, B.: A synthesis of cloud condensation nuclei
784 counter (CCNC) measurements within the EUCAARI network, *Atmos. Chem. Phys.*, 15, 12211–12229,
785 <https://doi.org/10.5194/acp-15-12211-2015>, 2015.

786 Petters, M. D. and Kreidenweis, S. M.: A single parameter representation of hygroscopic growth and cloud condensation
787 nucleus activity, *Atmos. Chem. Phys.*, 7, 1961–1971, <https://doi.org/10.5194/acp-7-1961-2007>, 2007.

788 Pringle, K. J., Tost, H., Pozzer, A., Pöschl, U., and Lelieveld, J.: Global distribution of the effective aerosol hygroscopicity
789 parameter for CCN activation, *Atmos. Chem. Phys.*, 10, 5241–5255, <https://doi.org/10.1007/978-0-306-48100-010.5194/acp-10-5241-2010>, 2010.

790 Pruppacher, H. R. and Klett, J. D.: *Microphysics of clouds and precipitation*, Kluwer, Dordrecht,
791 <https://doi.org/10.1007/978-0-306-48100-0>, 2000.

792 Rissler, J., Svenningsson, B., Fors, E. O., Bilde, M., and Swietlicki, E.: An evaluation and comparison of cloud condensation
793 nucleus activity models: Predicting particle critical saturation from growth at subsaturation, *J. Geophys. Res.*, 115,
794 22208, <https://doi.org/10.1029/2010JD014391>, 2010.

795 Roberts, G. and Nenes, A.: A continuous-flow streamwise thermal-gradient CCN chamber for atmospheric measurements,
796 *Aerosol Sci. Tech.*, 39, 206–221, <https://doi.org/10.1080/027868290913988>, 2005.

797 Rose, D., Gunthe, S. S., Mikhailov, E., Frank, G. P., Dusek, U., Andreae, M. O., and Pöschl, U.: Calibration and
798 measurement uncertainties of a continuous-flow cloud condensation nuclei counter (DMT-CCNC): CCN activation of
799 ammonium sulfate and sodium chloride aerosol particles in theory and experiment, *Atmos. Chem. Phys.*, 8, 1153–1179,
800 <https://doi.org/10.5194/acp-8-1153-2008>, 2008.

801 Rose, D., Nowak, A., Achtert, P., Wiedensohler, A., Hu, M., Shao, M., Zhang, Y., Andreae, M. O., and Pöschl, U.: Cloud
802 condensation nuclei in polluted air and biomass burning smoke near the mega-city Guangzhou, China – Part 1: Size-
803 resolved measurements and implications for the modeling of aerosol particle hygroscopicity and CCN activity, *Atmos.*
804 *Chem. Phys.*, 10, 3365–3383, <https://doi.org/10.5194/acp-10-3365-2010>, 2010.

805 Rose, D., Gunthe, S. S., Su, H., Garland, R. M., Yang, H., Berghof, M., Cheng, Y. F., Wehner, B., Achtert, P., Nowak, A.,
806 Wiedensohler, A., Takegawa, N., Kondo, Y., Hu, M., Zhang, Y., Andreae, M. O., and Pöschl, U.: Cloud condensation
807 nuclei in polluted air and biomass burning smoke near the mega-city Guangzhou, China – Part 2: Size-resolved aerosol
808 chemical composition, diurnal cycles, and externally mixed weakly CCN-active soot particles, *Atmos. Chem. Phys.*, 11,
809 2817–2836, <https://doi.org/10.5194/acp-11-2817-2011>, 2011.

811 Rosenfeld, D., Lohmann, U., Raga, G. B., O'Dowd, C. D., Kulmala, M., Fuzzi, S., Reissell, A., and Andreae, M. O.: Flood
812 or drought: How do aerosols affect precipitations?, *Science*, 321, <https://doi.org/1309-1313>, 10.1126/science.1160606,
813 2008.

814 Rosenfeld, D., Andreae, M. O., Asmi, A., Chin, M., de Leeuw, G., Donovan, D. P., Kahn, R., Kinne, S., Kivekäs, N.,
815 Kulmala, M., Lau, W. Sebastian Schmidt, K., Suni, T., Wagner, T., and Wild, M.: Global observations of aerosol-cloud-
816 precipitation-climate interactions, *Rev. Geophys.*, 52, 750–808, <https://doi.org/10.1002/2013RG000441>, 2014.

817 Salma, I., Ocskay, R., Varga, I., and Maenhaut, W.: Surface tension of atmospheric humic-like substances in connection with
818 relaxation, dilution, and solution pH, *J. Geophys. Res.*, 111, D23205, <https://doi.org/10.1029/2005JD007015>, 2006.

819 Salma, I., Ocskay, R., Chi, X., and Maenhaut, W.: Sampling artefacts, concentration and chemical composition of fine
820 water-soluble organic carbon and humic-like substances in a continental urban atmospheric environment, *Atmos.*
821 *Environ.*, 41, 4106–4118, <https://doi.org/10.1016/j.atmosenv.2007.01.027>, 2007.

822 Salma, I., Borsós, T., Weidinger, T., Aalto, P., Hussein, T., Dal Maso, M., and Kulmala, M.: Production, growth and
823 properties of ultrafine atmospheric aerosol particles in an urban environment, *Atmos. Chem. Phys.*, 11, 1339–1353,
824 <https://doi.org/10.5194/acp-11-1339-2011>, 2011.

825 Salma, I., Borsós, T., Németh, Z., Weidinger, T., Aalto, T., and Kulmala, M.: Comparative study of ultrafine atmospheric
826 aerosol within a city, *Atmos. Environ.*, 92, 154–161, <https://doi.org/10.1016/j.atmosenv.2014.04.020>, 2014.

827 Salma, I., Németh, Z., Weidinger, T., Kovács, B., and Kristóf, G.: Measurement, growth types and shrinkage of newly
828 formed aerosol particles at an urban research platform, *Atmos. Chem. Phys.*, 16, 7837–7851, <https://doi.org/10.5194/acp-16-7837-2016>, 2016.

829 Salma, I., Varga, V., and Németh, Z.: Quantification of an atmospheric nucleation and growth process as a single source of
830 aerosol particles in a city, *Atmos. Chem. Phys.*, 17, 15007–15017, <https://doi.org/10.5194/acp-17-15007-2017>, 2017.

831 Salma, I., Vasanits-Zsigrai, A., Machon, A., Varga, T., Major, I., Gergely, V., and Molnár, M.: Fossil fuel combustion,
832 biomass burning and biogenic sources of fine carbonaceous aerosol in the Carpathian Basin, *Atmos. Chem. Phys.*, 20,
833 4295–4312, <https://doi.org/10.5194/acp-20-4295-2020>, 2020a.

834 Salma, I., Vörösmarty, M., Gyöngyösi, A. Z., Thén, W., and Weidinger, T.: What can we learn about urban air quality with
835 regard to the first outbreak of the COVID-19 pandemic? A case study from central Europe, *Atmos. Chem. Phys.*, 20,
836 15725–15742, <https://doi.org/10.5194/acp-20-15725-2020>, 2020b.

837 Schmale, J., Henning, S., Henzing, B., Keskinen, H., Sellegri, K., Ovadnevaite, J., Bougiatioti, A., Kalivitis, N., Stavroulas,
838 I., Jefferson, A., Park, M., Schlag, P., Kristensson, A., Iwamoto, Y., Pringle, K., Reddington, C., Aalto, P., Äijälä, M.,
839 Baltensperger, U., Bialek, J., Birmili, W., Bukowiecki, N., Ehn, M., Fjæraa, A. M., Fiebig, M., Frank, G., Fröhlich, R.,
840 Frumau, A., Furuya, M., Hammer, E., Heikkinen, L., Herrmann, E., Holzinger, R., Hyono, H., Kanakidou, M., Kiendler-
841 Scharr, A., Kinouchi, K., Kos, G., Kulmala, M., Mihalopoulos, N., Motos, G., Nenes, A., O'Dowd, C., Paramonov, M.,
842 Petäjä, T., Picard, D., Poulain, L., Prévôt, A. S. H., Slowik, J., Sonntag, A., Swietlicki, E., Svenningsson, B., Tsurumaru,
843 H., Wiedensohler, A., Wittbom, C., Ogren, J. A., Matsuki, A., Yum, S. S., Myhre, C. L., Carslaw, K., Stratmann, F., and
844 Gysel, M.: Collocated observations of cloud condensation nuclei, particle size distributions, and chemical composition,
845 *Scient. Data*, 4, 170003, <https://doi.org/10.1038/sdata.2017.3>, 2017.

846 Schmale, J., Henning, S., Decesari, S., Henzing, B., Keskinen, H., Sellegri, K., Ovadnevaite, J., Pöhlker, M. L., Brito, J.,
847 Bougiatioti, A., Kristensson, A., Kalivitis, N., Stavroulas, I., Carbone, S., Jefferson, A., Park, M., Schlag, P., Iwamoto,
848 Y., Aalto, P., Äijälä, M., Bukowiecki, N., Ehn, M., Frank, G., Fröhlich, R., Frumau, A., Herrmann, E., Herrmann, H.,
849 Holzinger, R., Kos, G., Kulmala, M., Mihalopoulos, N., Nenes, A., O'Dowd, C., Petäjä, T., Picard, D., Pöhlker, C.,
850 Pöschl, U., Poulain, L., Prévôt, A. S. H., Swietlicki, E., Andreae, M. O., Artaxo, P., Wiedensohler, A., Ogren, J.,
851 Matsuki, A., Yum, S. S., Stratmann, F., Baltensperger, U., and Gysel, M.: Long-term cloud condensation nuclei number
852 concentration, particle number size distribution and chemical composition measurements at regionally representative
853 observatories, *Atmos. Chem. Phys.*, 18, 2853–2881, <https://doi.org/10.5194/acp-18-2853-2018>, 2018.

854 Sihto, S.-L., Mikkilä, J., Vanhanen, J., Ehn, M., Liao, L., Lehtipalo, K., Aalto, P. P., Duplissy, J., Petäjä, T., Kerminen, V.-
855 M., Boy, M., and Kulmala, M.: Seasonal variation of CCN concentrations and aerosol activation properties in boreal
856 forest, *Atmos. Chem. Phys.*, 11, 13269–13285, <https://doi.org/10.5194/acp-11-13269-2011>, 2011.

857 Sorjamaa, R., Svenningsson, B., Raatikainen, T., Henning, S., Bilde, M., and Laaksonen, A.: The role of surfactants in
858 Köhler theory reconsidered, *Atmos. Chem. Phys.*, 4, 2107–2117, <https://doi.org/10.1007/978-0-306-48100-010.5194/acp-4-2107-2004>, 2004.

859 Topping, D. O. and McFiggans, G.: Tight coupling of particle size, number and composition in atmospheric cloud droplet
860 activation, *Atmos. Chem. Phys.*, 12, 3253–3260, <https://doi.org/10.5194/acp-12-3253-2012>, 2012.

861 Wex, H., McFiggans, G., Henning, S., and Stratmann, F.: Influence of the external mixing state of atmospheric aerosol on
862 derived CCN number concentrations, *Geophys. Res. Lett.*, 37, 10805, <https://doi.org/10.1029/2010GL043337>, 2010.

863 Wiedensohler, A., Birmili, W., Nowak, A., Sonntag, A., Weinhold, K., Merkel, M., Wehner, B., Tuch, T., Pfeifer, S., Fiebig,
864 M., Fjæraa, A. M., Asmi, E., Sellegri, K., Depuy, R., Venzac, H., Villani, P., Laj, P., Aalto, P., Ogren, J. A., Swietlicki,
865 E., Williams, P., Roldin, P., Quincey, P., Hüglin, C., Fierz-Schmidhauser, R., Gysel, M., Weingartner, E., Riccobono, F.,
866 Santos, S., Grünig, C., Faloon, K., Beddows, D., Harrison, R., Monahan, C., Jennings, S. G., O'Dowd, C. D., Marinoni,
867 A., Horn, H.-G., Keck, L., Jiang, J., Scheckman, J., McMurry, P. H., Deng, Z., Zhao, C. S., Moerman, M., Henzing, B.,
868 de Leeuw, G., Löschau, G., and Bastian, S.: Mobility particle size spectrometers: harmonization of technical standards
869 and data structure to facilitate high quality long-term observations of atmospheric particle number size distributions,
870 *Atmos. Meas. Tech.*, 5, 657–685, <https://doi.org/10.5194/amt-5-657-2012>, 2012.